Kibble-Zurek behavior in one-dimensional disordered topological insulators

Zhoujian Sun, Menghua Deng, and Fuxiang Li*
School of Physics and Electronics, Hunan University, Changsha 410082, China

(Received 14 September 2022; revised 28 September 2022; accepted 28 September 2022; published 10 October 2022)

The discovery of nonlocal order parameters in real space provides a feasible scheme for studying dynamical critical behavior in topological systems. We study the critical phenomena in the one-dimensional Su-Schrieffer-Heeger (SSH) model by investigating the inhomogeneities in the local winding number in real space. By slowly quenching the system across the topological phase transition during a finite time interval, we find that the length scale defined through the local winding number satisfies the Kibble-Zurek mechanism. In contrast to the density of excitation, the scaling of this length scale is in full analog to the behavior of traditional continuous phase transitions with local order parameter and spontaneous symmetry breaking. In addition, the critical behavior and Kibble-Zurek mechanism in the generalized SSH with next-nearest-neighbor hopping are also studied. These results extend our understanding to the Kibble-Zurek mechanism and topological phase transition in nonequilibrium.

DOI: 10.1103/PhysRevB.106.134203

I. INTRODUCTION

Over the past few decades, topological insulators, as one of the mainstream research directions in condensed matter physics, have attracted much attention because of the fundamental interest and potential applications in nanoelectronics [1–6]. Topological quantum phases are characterized by a bulk topological invariant and accompanying protected boundary modes, whose description is beyond the scope of the traditional Landau-Ginzburg-Wilson framework in the language of local order parameters and spontaneous symmetry breaking [7–9]. Topological insulators possess edge states that propagate along a unidirection and are immune to the scattering of disorders [10]. In recent years, much attention has been paid to the study of novel dynamical topological properties in nonequilibrium dynamics in both theory and experiment [11–14].

As a general theory relating the phase transition and nonequilibrium dynamics, the famous Kibble-Zurek mechanism (KZM) was proposed and has been examined in diverse systems, ranging from superfluids [15–17] to superconductors [18–21], quantum Ising chains [22–25], ion crystals [26–28], Bose gases [29–33], and cosmological scenarios [34–36]. The KZM predicts that the number of topological defects generated exhibits a universal scaling behavior in a nonequilibrium system driven through a continuous phase transition during a finite time interval. It was first proposed by Kibble as a cosmological theory to describe the formation of the early universe [37], and subsequently applied to condensed matter systems by Zurek [38]. The central ideal of this theory is as follows. As slowly quenched across the critical transition point, the system experiences different dynamical stages. At initial stage far away from the critical point, the relaxation time is short and the state can adiabatically follow the ground state of the system. As approaching to the critical point at which the relaxation time diverges, the dynamics are no longer adiabatic and the system arrives at the impulse (diabatic) region. When system is far from the critical point again, the adiabatic evolution can be recovered. The moment at which the system fails to evolve adiabatically is called the freeze-out time. The freeze-out time $\hat{t}$ and the corresponding correlation length $\xi(\hat{t})$ can be determined as $\hat{t} \sim \tau_Q^{z\nu/1+z\nu}$ and $\xi(\hat{t}) \sim \tau_Q^{\nu/1+z\nu}$ [39], where τ_Q is the quench time and z and ν are both the critical exponents. Relevant physical quantities, such as topological defects, of the postquench system are simply determined by the correlation length at freeze-out time.

The KZM has also been studied in topological systems, in which the number of excitations is shown to satisfy the KZM [40–44]. However, this kind of simple generalization does not reveal the underlying physics of the topological nature. Topological phase transitions have no spontaneously broken symmetry, and no local order parameter as required in Landau's phase transition theory. It is worthy to ask whether the above freeze-out argument of the KZM works in topological systems that are described by a quantized nonlocal topological invariant. A breakthrough in this research direction was made recently in Ref. [45], in which the KZM was directly revealed in real space in a Chern insulator with weak disorder. By introducing the so-called local Chern marker as a local indicator of the topological phase [46–48], the authors find that a characteristic length scale can be defined in the inhomogeneities in the local Chern marker. The scaling behavior of this length scale is shown to follow the KZM, thus establishing an almost full analog to the dynamical critical behavior of systems with spontaneously broken symmetry and local order parameter. However, this study was constrained to the case of the two-dimensional (2D) Chern insulator whose topological invariant is the Chern number. One may wonder whether the KZM is still applicable in other types of topological systems, such as the 1D system that is described by a winding number.

*Corresponding author: fuxiangli@hnu.edu.cn

 ©2022 American Physical Society

In 1D topological systems protected by chiral symmetry, it was found that the winding number can also be represented in real space [47]. This representation is proven to be valid and convenient for exploring the disordered topological Anderson insulator. Such a real-space representation of the winding number was further modified by deriving the real-space winding number in view of the skew polarization [48].

In this paper, by defining a local indicator of winding number in real space, we systematically study the Kibble-Zurek mechanism in the 1D Su-Schrieffer-Heeger (SSH) model. We first find that this local winding indicator gives rise to a length scale that diverges near the critical transition point $\hat{\xi} \sim |t - t_c|^{-1}$ in equilibrium. By slowly quenching the system across the topological phase transition point during a finite time interval τ_Q, one also finds that the critical length scale satisfies the KZM: $\xi(\hat{t}) \sim \tau_Q^{\beta}$ with critical exponent $\beta = 1/2$. This scaling is in full analog to the behavior for the system undergoing a symmetry-breaking second-order phase transition. Moreover, we find that our results are not restricted to the simple short-range SSH models, but can be generalized to the long-range SSH model.

The paper is organized as follows. In Sec. II, we present the model and give a brief review of the calculation of the winding number. In Sec. III we show the critical phenomenon of the ground state in momentum space and in real space. In Sec. IV we study the KZM under slow quench protocol. In Sec. V we consider the long-range SSH model. Our conclusions are given in Sec. VI.

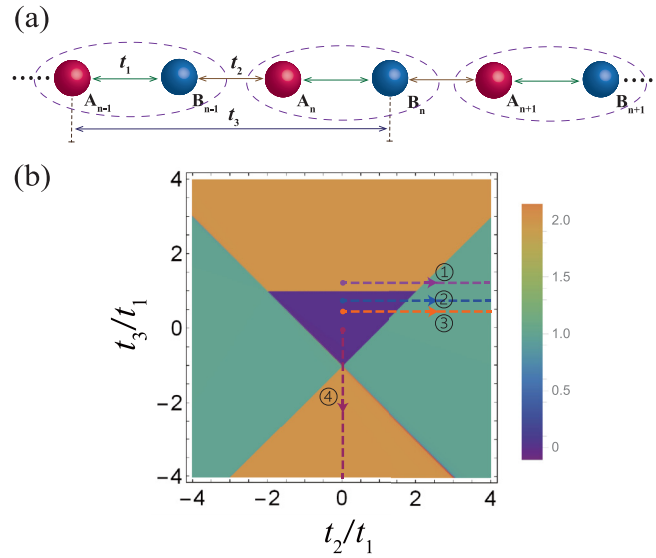

FIG. 1. (a) Schematic illustration of 1D SSH lattice. The system consists of two sublattices denoted by blue (A sublattice) and red (B sublattice) spheres, respectively. The dotted purple ellipse indicates the unit cell. (b) Phase diagram of the generalized SSH model. The winding number (shown by the color scale) is calculated as a function of t_2, t_3 in k space. Four dashed lines are displayed in different colors, which represent four different quench paths. The quench directions are indicated by the arrows. For paths ①–③, we quench t_2 from 0 to 60 with t_3 being 1.3, 0.6, and 0.4, respectively. In path ④, we fix $t_2 = 0$ and quench t_3 from 0 to -60. $t_1 = 1$ for all the paths.

II. THE MODEL

Without loss of generality, we take the 1D SSH model as an example to study the Kibble-Zurek mechanism. As shown in Fig. 1(a), in addition to the nearest-neighbor hopping terms t_1 (intracell) and t_2 (intercell), we also consider the next-nearest-neighbor (NNN) intercell hopping t_3. The SSH model is one of the most studied topological models that support nontrivial topological phases. When $t_3 = 0$, the system undergoes a topological phase transition from a topologically trivial phase for $t_1 > t_2$ to topologically nontrivial phase for $t_1 < t_2$ with $t_1 = t_2$ being the critical point. This topological phase transition can be described by a quantized nonlocal topological invariant, the winding number. The winding number can take values of 0 and ± 1, corresponding to the topologically trivial and nontrivial phases, respectively. When the NNN intercell hopping t_3 is nonzero, the phase diagram is more complex with a topologically nontrivial phase of winding number 2, as shown in Fig. 1(b).

We start the discussion with the tight-binding Hamiltonian:

$$\begin{aligned} H_r = &(t_1 + \Delta t_n) \sum_{n=1}^{N} |n\rangle\langle n| \otimes \boldsymbol{\sigma}_x \\ &+ t_2 \sum_{n=1}^{N-1} \left(|n+1\rangle\langle n| \otimes \frac{\boldsymbol{\sigma}_+}{2} + \text{H.c.} \right) \\ &+ t_3 \sum_{n=1}^{N-2} \left(|n+2\rangle\langle n| \otimes \frac{\boldsymbol{\sigma}_+}{2} + \text{H.c.} \right), \end{aligned} \tag{1}$$

where $\boldsymbol{\sigma}_\pm = \boldsymbol{\sigma}_x \pm i\boldsymbol{\sigma}_y$ and $\boldsymbol{\sigma}_{x,y,z}$ is the Pauli matrices acting on the two sublattices. n denotes the nth unit cell and N is the total number of unit cells. The open boundary condition is adopted in the calculations. In addition, we also introduce a weak-disorder term Δt_n in the nearest-neighbor intracell hopping t_1. Specifically, Δt_n is chosen to be uncorrelated and uniformly distributed in the interval $\{-\Delta t, \Delta t\}$. The strength of the disorder is weak enough that the Anderson localization length is much longer than the system size.

In the clean limit, the tight-binding Hamiltonian (1) can be diagonalized by making a Fourier transformation [49] and one can express the Hamiltonian in the momentum space in terms of Pauli matrices [50]:

$$\begin{aligned} \mathcal{H}_k = &(t_1 + t_2 \cos k + t_3 \cos 2k)\sigma_x \\ &+ (t_2 \sin k + t_3 \sin 2k)\sigma_y. \end{aligned} \tag{2}$$

Note that the Hamiltonian has no σ_z terms, and thus possesses the chiral symmetry $\sigma_z \mathcal{H}_k \sigma_z^{-1} = -\mathcal{H}_k$. The eigenvalues $E_\pm$ and eigenstates $|\psi_\pm\rangle$ can be readily obtained. By using the eigenstate of the valence band, one can get the Berry connection via $A_k = i\langle\psi_-|\partial_k|\psi_-\rangle$. Then the winding number in k space can be calculated by

$$w_k = \frac{1}{\pi} \oint_{\text{BZ}} A_k dk. \tag{3}$$

Here, "BZ" denotes that the integration is taken in the first Brillouin zone.

In the case with weak disorder, the translational symmetry is broken and the winding number defined in Eq. (3) does not

apply. Instead, the topological invariant can be defined in real space. One can calculate the corresponding winding number of a 1D system with chiral symmetry directly from the real space as proposed by Ref. [47]:

$$W_r = \mathrm{Tr}\, w(r), \quad \text{with} \quad w = Q_{12}[X, Q_{21}]. \tag{4}$$

Here, $w(r)$ is the local indicator of winding number. "Tr" refers to taking the trace over the real space. To calculate the local indicator w, one needs to define a homotopically equivalent flat-band Hamiltonian $Q = P_+ - P_-$, where $P_\pm$ are the projectors onto the conduction and valence bands, respectively. Then we define $Q_{12} = \Gamma_1 Q \Gamma_2$, $Q_{21} = \Gamma_2 Q \Gamma_1$, where $\Gamma_{1,2}$ are the projectors onto the two sublattice subspaces. X is the position operator. The chiral symmetry of the Hamiltonian is now expressed as $\Gamma \mathcal{H}_r \Gamma^{-1} = -\mathcal{H}_r$, where the chiral symmetry operator is $\Gamma = \Gamma_1 - \Gamma_2$. The real-space formula of the winding number is still valid even in the presence of disorder as long as the chiral symmetry is preserved.

III. THE CRITICAL PHENOMENON IN EQUILIBRIUM

In the continuous phase transitions of Landau-Wilson type, all relevant physical quantities, like the order parameter, specific heat, susceptibility, and correlation length, exhibit universal scaling behaviors as approaching the critical point. Topological phase transitions, however, are characterized not by local order parameter, but by a nonlocal topological invariant, and thus cannot be described in terms of Landau-Wilson theory. It is necessary to study whether similar critical phenomena are present in a topological system. Based on the local winding number indicator given in the above section, we will define a correlation length as the size of inhomogeneities of the local indicator, and study its critical behaviors.

A. In the clean system

In the clean system (2), the winding number is expressed as an integration of Berry connection A_k over the first Brillouin zone (3). Thus one can focus on the Berry connection A_k and investigate its profile in the momentum space, from which a length scale can be derived and treated as a local parameter. Note that a similar procedure was taken to study the critical behavior of Berry curvature in a Chern insulator [45].

In Fig. 2, we present the results of the Berry connection of a 1D topological model in the ground state. By fixing $t_2 = 1$, six different values of control parameter t_1 are plotted in the region near $k = \pi$ in Fig. 2(a). One observes that there is a peak of Berry connection around $k = \pi$. The peak first grows with the control parameter t_1, reaches the maximum value at phase transition point $t_1 = 1$, and then decreases. One can find that there may exist a critical behavior around the transition point.

To quantitatively describe the critical behavior, we define a correlation length ξ_k by the inverse of the full width at half maximum of Berry connection A_k. The calculation method is given in the Appendix. In Fig. 2(b) we plot the correlation length ξ_k in k space as a function of parameter t_1. As the system approaches the critical point $t_c = 1$, one observes that the correlation length diverges. We further plot the ξ_k as a function of $|t_1 - t_c|$ in the log-log scale in Fig. 2(c). One can

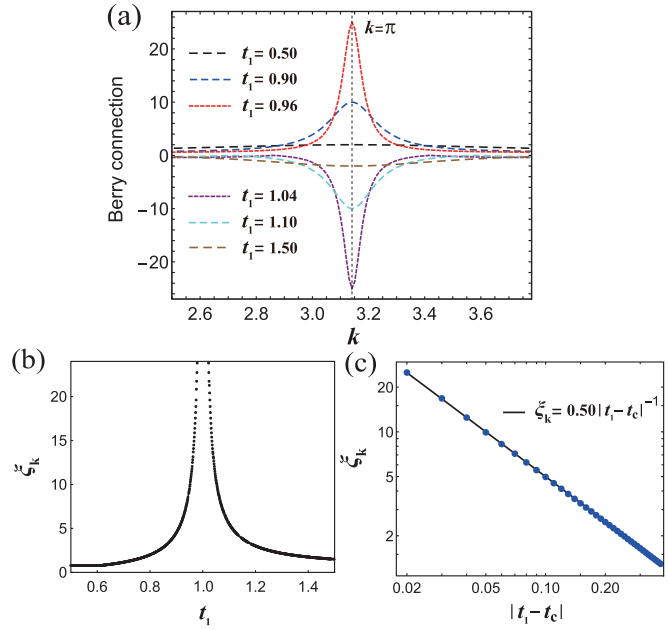

FIG. 2. Berry connection of the SSH model in the interval $2.5 \leqslant k \leqslant 3.78$ from $t_1 = 0.5$ (topology) to $t_1 = 1.5$ (trivial) for (a). In this case we set $t_2 = 1$ and $t_3 = 0$. (b) The correlation length in k space ξ_k as a function of control parameter t_1 when it crosses the critical point $t_c = 1$. ξ_k as a function of $|t_1 - t_c|$ in the log-log scale is plotted in (c). Black line shows fit to blue dots coming from numerics.

see that the correlation length ξ_k scales with parameter $|t_1 - t_c|$ as $\xi_k \sim |t_1 - t_c|^{-\nu}$ with critical exponent $\nu = 1$ [45].

Actually, one can analytically determine the correlation length exponent. For simplicity, considering the case of $t_3 = 0$, the Berry connection can be explicitly given as

$$A_k = \frac{t_2(t_2 + t_1 \cos k)}{2(t_1 + t_2 \cos k)^2 + (t_2 \sin k)^2}. \tag{5}$$

Near the point $k = \pi$, by writing $t_1 = 1 + \delta t, t_2 = 1, k = \pi + \delta k$, one can obtain $A_k \sim \frac{-\delta t + (\delta k)^2}{(\delta t)^2 + (\delta k)^2}$ and $A_\pi \sim -\frac{1}{\delta t}$. From the denominator, one can see that the full width at half maximum of A_k occurs at $\delta k_c \sim \delta t$. Thus the correlation length is $\xi_k \sim \frac{1}{\delta k_c} \sim (\delta t)^{-1}$ with the critical exponent being 1.

B. With weak disorder

Next, we turn to the case with disorder (1) and study the critical behavior in terms of the local winding number (4) in real space. Because of the presence of weak disorder, the local winding number in real space is no longer a constant value, but fluctuates at different positions. In this case, one can obtain the correlation length ξ_r in real space from the disorder-averaged autocovariance function as it drops below zero (see Appendix).

As shown in Figs. 3(a1)–3(a5), we present the distribution of the local winding number at each site for different values of parameter t_1 around the transition point. The system size is $N = 250$ and open boundary conditions are considered. One can find that the correlation length ξ_r increases as the parameter t_1 approaches the critical point. Naturally, we show the relation of the correlation length in real space ξ_r with

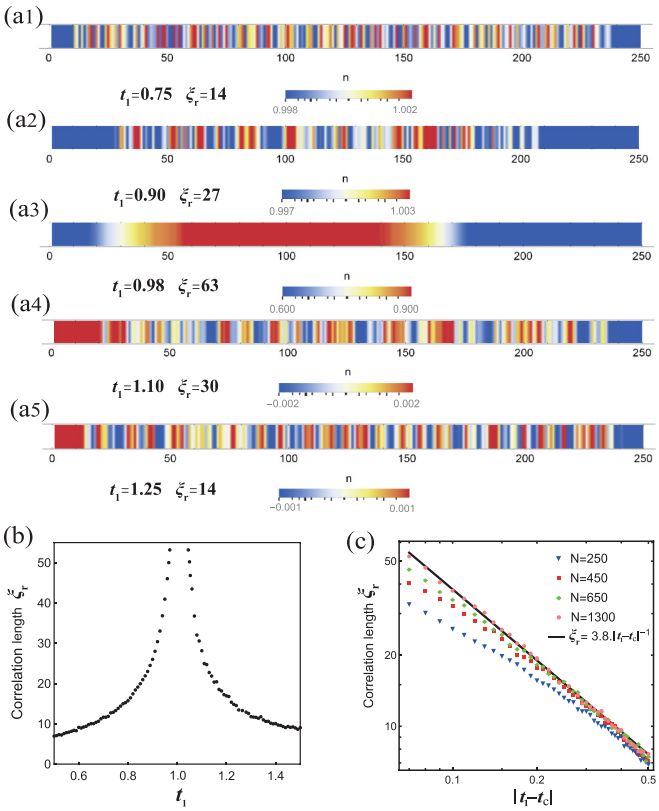

FIG. 3. (a1)–(a5) The distribution of local winding number across the critical point in disordered systems. The system size is $N = 250$ and the disorder amplitude is $\Delta t = 0.005$. The corresponding control parameter t_1 and the correlation length ξ_r of real space are marked under the corresponding figures. (b) The correlation length in real space ξ_r as a function of control parameter t_1 when it crosses the critical point $t_1 = 1$. (c) ξ_r as a function of $|t_1 - t_c|$ in the log-log scale for different system sizes ranging from $N = 250$ to $N = 1300$ and averaging is done over 50 random values of Δt_n.

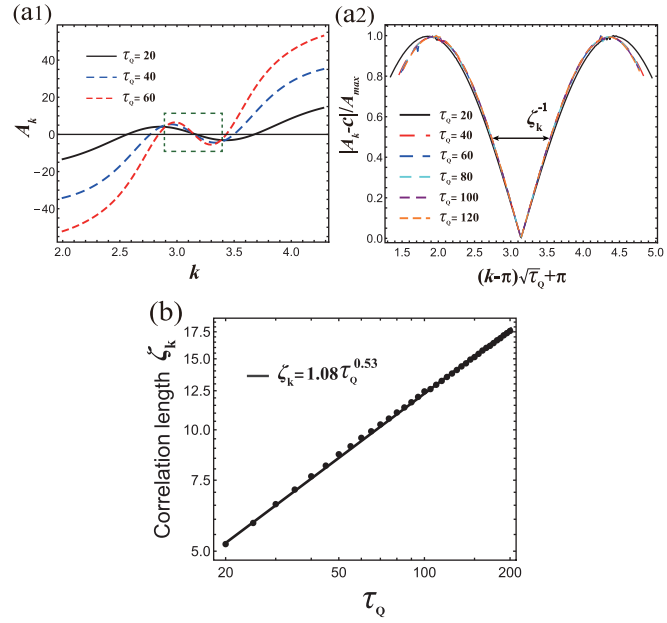

FIG. 4. (a1) Berry connection of SSH model after the end of the slow quench for three different τ_Q. The dashed green box is the region of interest near $k = \pi$. (a2) The Berry connection in the region near $k = \pi$ is plotted as a function of $(k - \pi)\sqrt{\tau_Q} + \pi$ for different values of τ_Q. Here, the vertical axis is subtracted a constant c, where $c = 0.5$. The black arrows indicate the inverse of defined correlation length ζ_k. (b) The correlation length in k space ζ_k as a function of quench time τ_Q in the log-log scale. The black line is a fitting with $\zeta_k = 1.08\tau_Q^{0.53}$.

the control parameter t_1 in Fig. 3(b), which exhibits a similar critical behavior with the k space. We further plot the ξ_r as a function of the average values of $|t_1 - t_c|$ in the topological regime in Fig. 3(c). Different system sizes are denoted with different colors. The larger the system size, the closer to 1 the correlation length exponent. The correlation length exponent in the disordered case is thus in agreement with what we find from the clear ones when the system size is large enough.

For the above discussions, we find that the critical phenomenon in the 1D topological phase transition does exist both in the momentum space and in the real space. In both cases, we obtain the same critical exponent $\nu = 1$ in the scaling of correlation length. In the next section, we study the critical behavior of topological systems under slow quench dynamics.

IV. KIBBLE-ZUREK MECHANISM UNDER SLOW QUENCH DYNAMICS

In this section, we study the quench dynamics of the 1D SSH model. We consider the slow quench protocol that the parameter t_1 is varied as $t_1(t) = t_0 \sin^2[(\pi/2)(t/\tau_Q)]$ with fixed $t_2 = 1$, $t_3 = 0$. As such, the system is quenched from the topological phase at initial time $t = 0$ to the trivial phase at final time $t = \tau_Q$. Here, we set $t_0 = 60$ in clean systems and $t_0 = 2$ in disorder systems; τ_Q determines the quench rate. The reason we adopt this protocol is to make sure that, at the initial time and final time, the system is not changed too abruptly as compared to linear quench protocol. One may think that the nonlinearity may modify the power-law behavior [51,52]. In fact, this protocol reduces to linear at a time near the phase transition point at $t = \tau_Q/2$. As long as the quenching time τ_Q is sufficiently large, this linear relation will be sustained in the impulse region of the nonadiabatic transition, and thus does not affect the power-law behavior.

In clean systems (2), we first evaluate the Berry connection A_k by using the final evolved wave functions after the slow quench dynamics, and then extract the corresponding correlation length. The Berry connection after the slow quench dynamics is shown in Fig. 4(a1) as a function of momentum k for three different values of quench time τ_Q. Here we only consider the region near $k = \pi$ as it determines the main form of Berry connection and the reason will be explained later by using an analytical model. The postquench form of the Berry connection near $k = \pi$ for different quench times is shown in Fig. 4(a2), in which we define the correlation length ζ_k by the inverse of the full width at half maximum of the Berry connection. For different quench rates, the Berry connection near $k = \pi$ collapses to one single line if we rescale the momentum k by a factor $\tau_Q^{1/2}$. We further plot the correlation

length ζ_k as a function of quench time τ_Q in the log-log scale as denoted by the black dots shown in Fig. 4(b). The scaling exponent of the black line is indeed near 0.5, which is in good agreement with the result of the Kibble-Zurek mechanism. Actually, according to the KZM, the size of inhomogeneities is given by $\xi(\hat{t}) = \tau_Q^{\nu/1+z\nu}$ with the exponent being 1/2 for the 1D SSH model, in which $\nu = z = 1$ are the correlation length and the dynamical critical exponent, respectively, as already obtained in previous sections.

Here, we can provide an analytical study of the evolved Berry connection under slow quench dynamics. We consider a slow quench protocol such as $t_1 = g/t$ with g being the quench rate, and keeping parameter $t_2 = 1$ as a constant. The quench time is from $t = 0$ to $t = \infty$, so that the system is quenched from an initial deep trivial phase to the final nontrivial phase. Specifically, we need to solve the following generalized Landau-Zener problem:

$$i\partial_t|\psi(t)\rangle = \hat{H}(t)|\psi(t)\rangle, \tag{6}$$

with the time-dependent Hamiltonian

$$\hat{H}(t) = \left(\frac{g}{t} + \cos k\right)\sigma_x + \sin k\sigma_y, \tag{7}$$

in which only the nearest-neighbor hopping is considered. If the system starts from the initial ground state, $|\psi(0)\rangle = \frac{1}{\sqrt{2}}(1,-1)^T$, then the final wave vector can be found to be [14]

$$|\psi(t)\rangle = e^{-i\varepsilon t+i\phi}\sqrt{P}|u_+\rangle + e^{i\varepsilon t}\sqrt{1-P}|u_-\rangle, \tag{8}$$

in which $\varepsilon = 1$ is the absolute value of eigenenergy after the slow quench, ϕ is an undetermined phase factor, and $u_\pm = \frac{1}{\sqrt{2}}(1,\pm e^{ik})^T$ is the instantaneous eigenvector of the Hamiltonian at time approaching infinity. The Landau-Zener transition probability P is

$$P = \frac{e^{-2\pi g\cos k} - e^{-2\pi g}}{e^{2\pi g} - e^{-2\pi g}}. \tag{9}$$

One can see that P takes its maximum at $k = \pi$, and quickly decreases to zero away from $k = \pi$. Using Eq. (8), one can readily obtain the time-dependent Berry connection $A_k(t)$:

$$A_k(t) = -(2P-1)(\partial_k\varepsilon)t + [PA_{++} + (1-P)A_{--}] + e^{2i\varepsilon t}\sqrt{P(1-P)}A_{+-} + e^{-2i\varepsilon t}\sqrt{P(1-P)}A_{-+}. \tag{10}$$

Here, we define the Berry connection tensor $A_{jl} = i\langle u_j|\partial_k u_l\rangle$ with $j, l = 1, 2$. For our case, the final Hamiltonian is simple, and we find that $A_{++} = A_{--} = -A_{+-} = -A_{-+} = 1/2$ independently of k. Therefore, the above expression can be further simplified. The first term is time-dependent. However, since in the final Hamiltonian, the band is flat and the eigenenergy ε is independent of k, this term vanishes. For a more general Hamiltonian, this term becomes important. Since eigenenergy always finds its minimum at $k = \pi$ leading to $\partial_k\varepsilon = 0$ near this point, this term vanishes near $k = \pi$. Away from $k = \pi$, however, $\partial_k\varepsilon$ becomes nonzero. This leads to a linear increase of this term. This argument explains why, in Fig. 4(a1), the Berry connection increases as one increases τ_Q. For the crossing terms with A_{+-} and A_{-+}, it is an oscillating term with

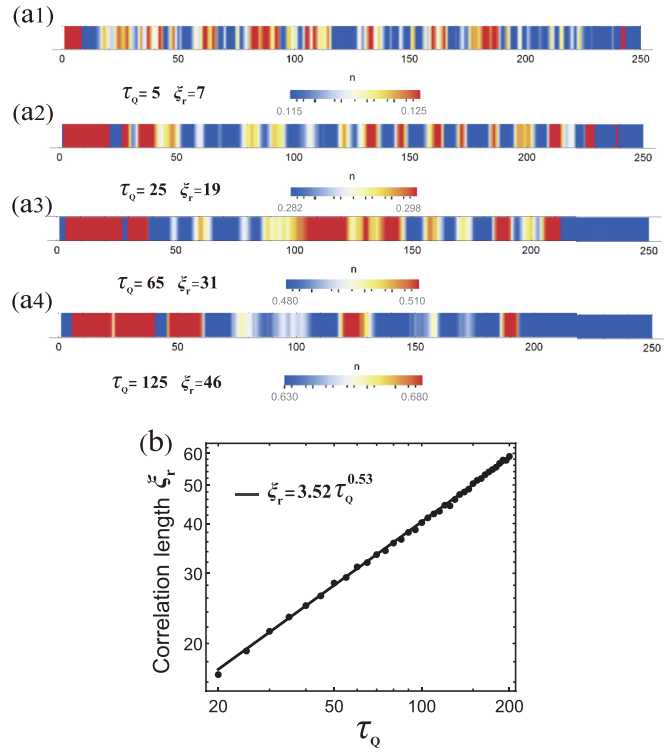

FIG. 5. (a1)–(a4) The distribution of local winding number at the end of the slow quench in disordered systems. The quench time ranges from $\tau_Q = 5$ to $\tau_Q = 125$, the system size is $N = 250$, and the disorder amplitude is $\Delta t = 0.005$. In (b), the correlation length in real space ξ_r as a function of quench time τ_Q in the log-log scale. The black line yields $\xi_r = 3.52\tau_Q^{0.53}$. The black dots are the numeric results. Here the lattice size $N = 500$, the disorder amplitude is $\Delta t = 0.005$, and averaging is done over 100 random values of Δt_n.

time. Its main form is determined by the factor $\sqrt{P(1-P)}$ of the LZ transition probability. Due to this factor, this crossing term quickly decreases to zero away from the $k = \pi$ point. The time-independent term is simply a constant of 1/2. From this simple analytical model, we see that the physically meaningful part of the Berry connection is located near $k = \pi$, from which the correlation length ζ_k should be defined.

Similarly to the clean system, we also obtain the final evolved wave functions after the slow quench dynamics in the disordered case (1). One finds that the postquench correlation length ξ_r that we defined to measure the inhomogeneities also increases with the quench time; see Figs. 5(a1)–5(a4). We further plot the correlation length ξ_r as a function of quench time τ_Q in the log-log scale in Fig. 5(b). One again finds that $\xi_r \sim \tau_Q^{0.5}$ with exponent being 0.5.

We note that, previously, the KZM has been studied in disordered systems. For example, in Ref. [23], the 1D random Ising spin model was studied, and it was found that the density of excitations has only logarithmic dependence on the transition rate. The reason is that the randomness of ferromagnetic couplings in the model changes the universality class with respect to the pure Ising chain. Any strength of disorder drives the 1D system into a localized regime, and thus the critical exponent is $\nu = 2$ and $z \to \infty$ rather than $\nu = 1$ and $z = 1$. Compared with our results, it shows that

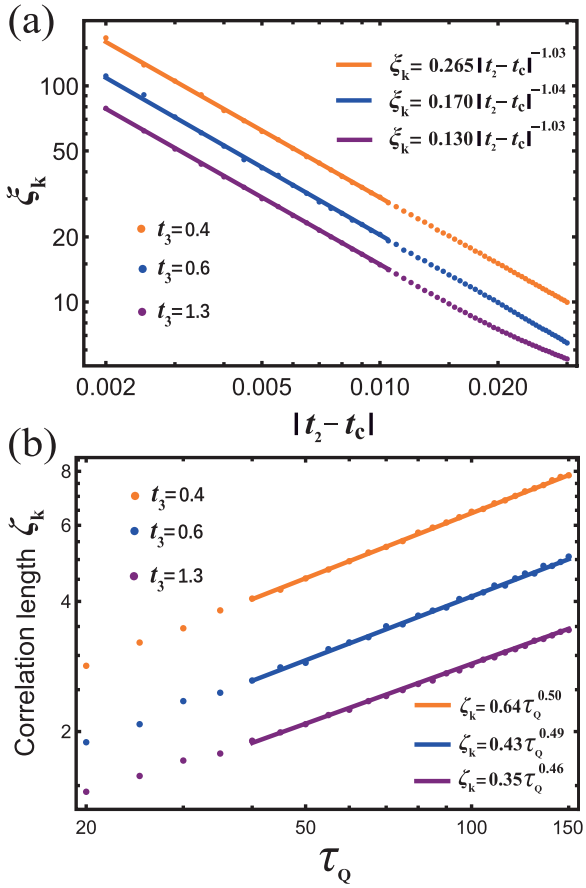

FIG. 6. In (a), for the system with next-nearest-neighbor hopping term t_3, the correlation length ξ_k in equilibrium as a function of $|t_2 - t_c|$ in the log-log scale is plotted. In (b), the correlation length at the end of the quench in k space ζ_k as a function of quench time τ_Q in the log-log scale for the long-range SSH model. The three colors correspond to the three quench paths ①–③ in the phase diagram.

disorder plays distinctive roles in topological systems and in nontopological systems. In our problem, we considered only weak disorder, and the scaling of the local winding number is the same as that in the pure system, which can be attributed to the topological nature that makes the behavior robust.

V. KIBBLE-ZUREK MECHANISM IN THE GENERALIZED SSH MODEL

Until now, the KZM has been validated in the standard SSH models. One may wonder whether this finding can also be extended to the other systems. In this section, we investigate the KZM in the generalized SSH model with the Hamiltonian given by Eqs. (1) and (2). As shown in Fig. 1(b), we first repeat the phase diagram of the generalized SSH model in k space [50]. We study four different quench paths as indicated in the phase diagram. The quench protocol is the same as that in previous sections. The quench path ① belongs to the $w = 2 \to 0$ case and the critical point is at $t_c = 2.3$. Quench paths ② and ③ are both $w = 0 \to 1$ phase transitions and the phase transition points t_c are 1.6 and 1.4 separately. The last quench path ④ is the $w = 0 \to 2$ phase transition, and the corresponding critical point is $t_c = -1$. Then we can study

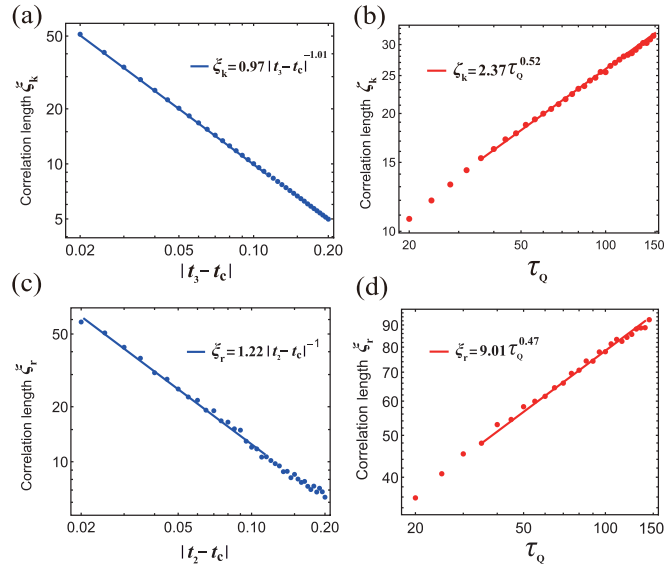

FIG. 7. For (a) and (b), the correlation length in k space along path ④ of the phase diagram. (a) The correlation length ξ_k in equilibrium as a function of $|t_3 - t_c|$ in the log-log scale. (b) The correlation length ζ_k vs quench time τ_Q in the log-log scale. For (c) and (d), the correlation length in real space along path ② of the phase diagram. We fix $t_1 = 1$, $t_3 = 0.4$, and quench t_2 from 0 to 4. We plot ξ_r vs $|t_2 - t_c|$ under the log-log scale in (c). ξ_r as a function of quench time τ_Q under the log-log scale is displayed in (d). Here the lattice size $N = 250$, the disorder amplitude is $\Delta t = 0.005$, and averaging is done over 100 random values of Δt_n. Blue and red lines are both fittings.

the change of correlation length in equilibrium states and slow quench along these paths.

In Fig. 6(a), we present the correlation length in equilibrium states near the phase transition point in paths ①–③ of Fig. 1(b). We find the correlation length decreases with $|t_2 - t_c|$ and exhibits a $\xi_k \propto |t_2 - t_c|^{-1}$ scaling from the fits for the results of three different colors. In Fig. 6(b), we plot the correlation length after the quench ζ_k vs quench time τ_Q in the log-log scale along quench paths ①–③ of the phase diagram. As quench time τ_Q increases, all three different quench paths exhibit scaling behaviors of correlation length with exponents being very close to 0.5.

To complete the results of Fig. 6, we also consider another quench path ④ and extend the quench path ② into the real space with disorder. As shown in Figs. 7(a) and 7(b), the same correlation length exponent $\nu = 1$ and the dynamic exponent $z = 1$ can be found in the case in which the system is quenching along $w = 0 \to 2$. In Figs. 7(c) and 7(d), we verify that the KZM can be also satisfied in the generalized SSH model from the view of real space. All of this demonstrates that, in the presence of the next-nearest-neighbor hopping term, the KZM in 1D topological insulators is still observable as a universal theory in physics.

VI. CONCLUSIONS

To conclude, we have studied the Berry connection and local winding number of the 1D SSH model in equilibrium states and slow quench circumstances. We found the critical

behaviors are present in both cases. After we defined the corresponding correlation length, we found the KZM can be observed in momentum space via the Berry connection and in real space by the local winding number. Moreover, we extend our results to the long-range systems. The critical exponents show good agreement with the predictions as given by the KZM.

ACKNOWLEDGMENTS

This work was supported by the National Key Research and Development Program of the Ministry of Science and Technology (Grant No. 2021YFA1200700), the National Natural Science Foundation of China (Grant No. 11905054 and No. 12275075), and the Fundamental Research Funds for the Central Universities of China.

APPENDIX: THE DEFINITION METHOD OF CORRELATION LENGTH

For the clean system, as shown in Fig. 8, we defined the correlation length under equilibrium states ξ_k by the inverse of width of black arrows in $|A_k/A_\pi| = 0.5$. A similarly defined method is made by Ref. [45].

In a randomized disorder system, the autocorrelation plot is a common tool for checking randomness of the data set. The autocorrelation coefficient is given by

$$\mathcal{R}_r = \frac{\mathcal{A}_r}{\mathcal{A}_0}. \tag{A1}$$

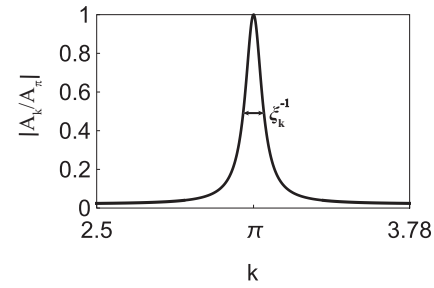

FIG. 8. The absolute value of Berry connection in the interval $2.5 \leqslant k \leqslant 3.78$ under equilibrium states. The marked black arrows denote the corresponding inverse of correlation length ξ_k.

The autocorrelation function $\mathcal{A}_r$ and the variance function $\mathcal{A}_0$ are expressed in

$$\mathcal{A}_r = \frac{1}{N}\sum_{x=1}^{N-r}(w_x - \overline{w})(w_{x+r} - \overline{w}), \tag{A2}$$

$$\mathcal{A}_0 = \frac{\sum_{x=1}^{N}(w_x - \overline{w})^2}{N}, \tag{A3}$$

where N is the length of the data set, x is the position order, r is the position lag, and $\overline{w}$ is the average of the data set. The autocorrelation coefficient is ranging from -1 to 1.

Similarly to the previous work, we defined the size of the inhomogeneities in the real space from the correlation length ξ_r by the distance between when the disorder-averaged autocorrelation coefficient first crosses zero ($\mathcal{R}_r = 0$).

[1] Y. Fan, P. Upadhyaya, X. Kou, M. Lang, S. Takei, Z. Wang, J. Tang, L. He, L.-T. Chang, M. Montazeri, G. Yu, W. Jiang, T. Nie, R. N. Schwartz, Y. Tserkovnyak, and K. L. Wang, Nat. Mater. **13**, 699 (2014).
[2] A. R. Mellnik, J. S. Lee, A. Richardella, J. L. Grab, P. J. Mintun, M. H. Fischer, A. Vaezi, A. Manchon, E.-A. Kim, N. Samarth, and D. C. Ralph, Nature (London) **511**, 449 (2014).
[3] W. Tian, W. Yu, J. Shi, and Y. Wang, Materials (Basel) **10**, 814 (2017).
[4] M. Z. Hasan and C. L. Kane, Rev. Mod. Phys. **82**, 3045 (2010).
[5] X. L. Qi and S. C. Zhang, Rev. Mod. Phys. **83**, 1057 (2011).
[6] Y. Hatsugai, Phys. Rev. Lett. **71**, 3697 (1993).
[7] D. J. Thouless, M. Kohmoto, M. P. Nightingale, and M. den Nijs, Phys. Rev. Lett. **49**, 405 (1982).
[8] M. McGinley and N. R. Cooper, Phys. Rev. Lett. **121**, 090401 (2018).
[9] Z.-H. Liu, O. Entin-Wohlman, A. Aharony, J. Q. You, and H. Q. Xu, Phys. Rev. B **104**, 085302 (2021).
[10] A. Coutant, V. Achilleos, O. Richoux, G. Theocharis, and V. Pagneux, Phys. Rev. B **102**, 214204 (2020).
[11] N. Fläschner, D. Vogel, M. Tarnowski, B. S. Rem, D. S. Luhmann, M. Heyl, J. C. Budich, L. Mathey, K. Sengstock, and C. Weitenberg, Nat. Phys. **14**, 265 (2018).
[12] L. D'Alessio and M. Rigol, Nat. Commun. **6**, 8336 (2015).
[13] P. Hauke, M. Lewenstein, and A. Eckardt, Phys. Rev. Lett. **113**, 045303 (2014).
[14] J. Ye and F. Li, Phys. Rev. A **102**, 042209 (2020).
[15] P. M. Chesler, A. M. Garcia-Garcia, and H. Liu, Phys. Rev. X **5**, 021015 (2015).
[16] B. Ko, J. W. Park, and Y.-I. Shin, Nat. Phys. **15**, 1227 (2019).
[17] L. Mathey and A. Polkovnikov, Phys. Rev. A **81**, 033605 (2010).
[18] J. Sonner, A. del Campo, and W. H. Zurek, Nat. Commun. **6**, 7406 (2015).
[19] J. Garaud and E. Babaev, Phys. Rev. Lett. **112**, 017003 (2014).
[20] R. Monaco, J. Mygind, M. Aaroe, R. J. Rivers, and V. P. Koshelets, Phys. Rev. Lett. **96**, 180604 (2006).
[21] N. Defenu, T. Enss, and J. C. Halimeh, Phys. Rev. B **100**, 014434 (2019).
[22] P. Silvi, G. Morigi, T. Calarco, and S. Montangero, Phys. Rev. Lett. **116**, 225701 (2016).
[23] J. Dziarmaga, Phys. Rev. B **74**, 064416 (2006).
[24] M. Kolodrubetz, B. K. Clark, and D. A. Huse, Phys. Rev. Lett. **109**, 015701 (2012).
[25] A. Sinha, D. Sadhukhan, M. M. Rams, and J. Dziarmaga, Phys. Rev. B **102**, 214203 (2020).
[26] S. Ulm, J. Rossnagel, G. Jacob, C. Degünther, S. T. Dawkins, U. G. Poschinger, R. Nigmatullin, A. Retzker, M. B. Plenio, F. Schmidt-Kaler, and K. Singer, Nat. Commun. **4**, 2290 (2013).
[27] K. Pyka, J. Keller, H. Partner, R. Nigmatullin, T. Burgermeister, D. M. Meier, K. Kuhlmann, A. Retzker, M. Plenio, W. Zurek, A. del Campo, and T. Mehlstäubler, Nat. Commun. **4**, 2291 (2013).

[28] M. Mielenz, J. Brox, S. Kahra, G. Leschhorn, M. Albert, T. Schaetz, H. Landa, and B. Reznik, Phys. Rev. Lett. **110**, 133004 (2013).
[29] J. Beugnon and N. Navon, J. Phys. B: At., Mol. Opt. Phys. **50**, 022002 (2017).
[30] A. L. Navon, N. Gaunt, R. P. Smith, and Z. Hadzibabic, Science **347**, 167 (2015).
[31] J. Goo, Y. Lim, and Y. Shin, Phys. Rev. Lett. **127**, 115701 (2021).
[32] L. Chomaz, L. Corman, T. Bienaimé, R. Desbuquois, C. Weitenberg, S. Nascimbène, J. Beugnon, and J. Dalibard, Nat. Commun. **6**, 6162 (2015).
[33] N. Navon, R. P. Smith, and Z. Hadzibabic, Nat. Phys. **17**, 1334 (2021).
[34] Y. M. Bunkov and O. D. Timofeevskaya, Phys. Rev. Lett. **80**, 4927 (1998).
[35] V. B. Eltsov, T. W. B. Kibble, M. Krusius, V. M. H. Ruutu, and G. E. Volovik, Phys. Rev. Lett. **85**, 4739 (2000).
[36] S. Casado, W. González-Viñas, S. Boccaletti, P. L. Ramazza, and H. Mancini, Eur. Phys. J.: Spec. Top. **146**, 87 (2007).
[37] T. W. B. Kibble, J. Phys. A: Math. Gen. **9**, 1387 (1976).
[38] W. H. Zurek, Nature (London) **317**, 505 (1985).
[39] A. del Campo and W. H. Zurek, Int. J. Mod. Phys. A **29**, 1430018 (2014).
[40] L. Ulčakar, J. Mravlje, A. Ramšak, and T. Rejec, Phys. Rev. B **97**, 195127 (2018).
[41] L. Ulčakar, J. Mravlje, and T. Rejec, Phys. Rev. B **100**, 125110 (2019).
[42] A. Dutta, R. R. P. Singh, and U. Divakaran, Europhys. Lett. **89**, 67001 (2010).
[43] M. Lee, S. Han, and M. S. Choi, Phys. Rev. B **92**, 035117 (2015).
[44] A. Bermudez, D. Patané, L. Amico, and M. A. Martin-Delgado, Phys. Rev. Lett. **102**, 135702 (2009).
[45] L. Ulčakar, J. Mravlje, and T. C. V. Rejec, Phys. Rev. Lett. **125**, 216601 (2020).
[46] R. Bianco and R. Resta, Phys. Rev. B **84**, 241106(R) (2011).
[47] I. Mondragon-Shem, T. L. Hughes, J. Song, and E. Prodan, Phys. Rev. Lett. **113**, 046802 (2014).
[48] L. Lin, Y. Ke, and C. Lee, Phys. Rev. B **103**, 224208 (2021).
[49] A. Dutta and A. Dutta, Phys. Rev. B **96**, 125113 (2017).
[50] H.-C. Hsu and T.-W. Chen, Phys. Rev. B **102**, 205425 (2020).
[51] R. Barankov and A. Polkovnikov, Phys. Rev. Lett. **101**, 076801 (2008).
[52] S. Mondal, K. Sengupta, and D. Sen, Phys. Rev. B **79**, 045128 (2009).